Volume 2
Number 2
February 2023
Pages 229–348

Energy Advances

rsc.li/energy-advances

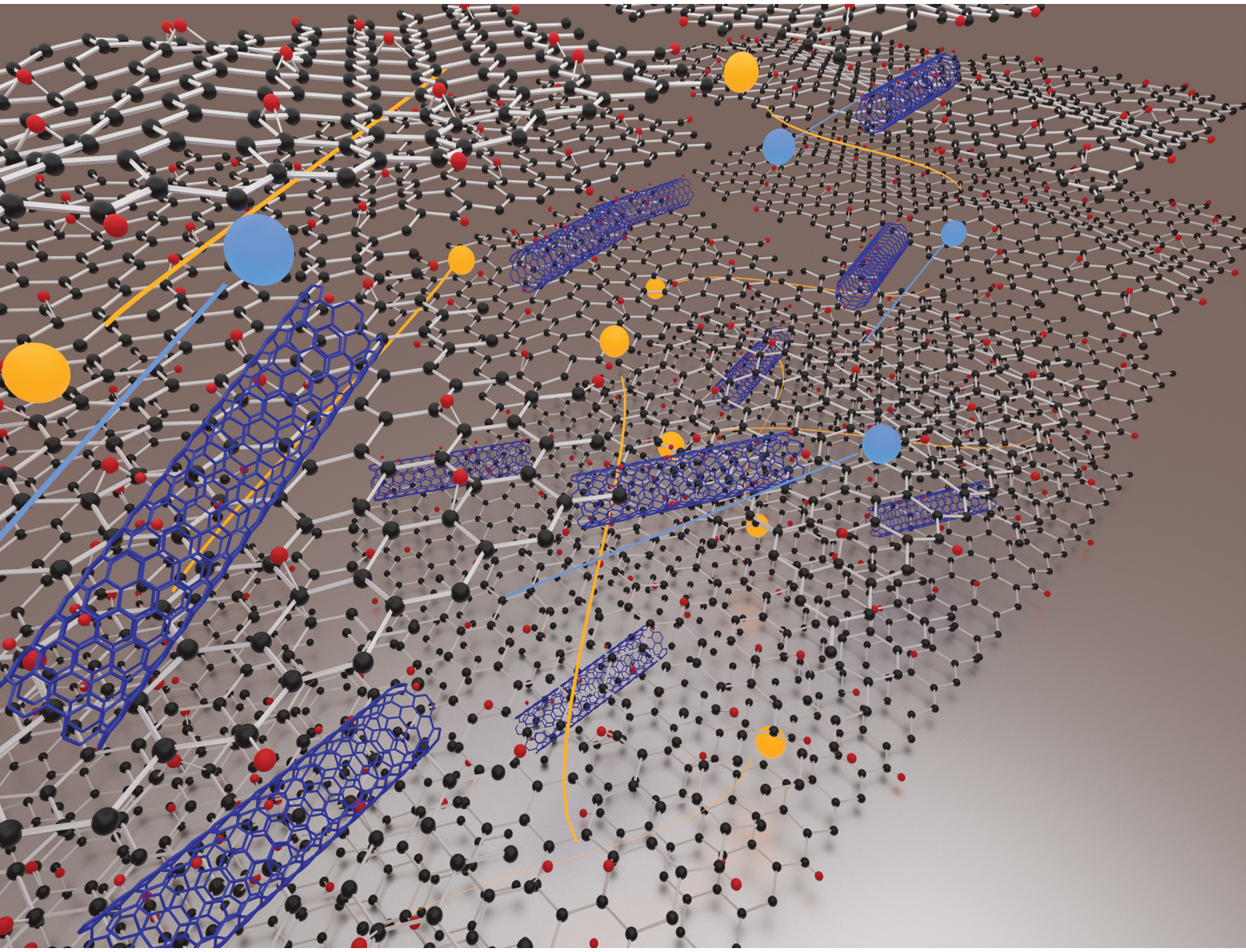

ISSN 2753-1457

ROYAL SOCIETY OF CHEMISTRY

COMMUNICATION
Shinya Hayami *et al.*
Free-standing graphene oxide/oxidized carbon nanotube films with mixed proton and electron conductor properties

Energy Advances

COMMUNICATION

View Article Online
View Journal | View Issue

Cite this: *Energy Adv.*, 2023, 2, 293

Received 16th November 2022,
Accepted 8th January 2023

DOI: 10.1039/d2ya00314g

rsc.li/energy-advances

Free-standing graphene oxide/oxidized carbon nanotube films with mixed proton and electron conductor properties†

Nurun Nahar Rabin,[ab] Md. Saidul Islam,[ab] Mohammad Atiqur Rahman,[b] Ryuta Tagawa,[b] Yuta Shudo,[c] Yoshihiro Sekine[bd] and Shinya Hayami*[abe]

Herein, a hybrid of graphene oxide and oxidized single-wall carbon nanotube (GO/Ox-SWCNT) free-standing film showing efficient mixed proton and electron conducting (MPEC) properties is demonstrated. The obtained proton and electronic conductivities are 5.24 × 10^{-3} and 1.35 × 10^{-3} S cm^{-1}, respectively. The ease of the GO/Ox-SWCNT free-standing film synthesis process along with the excellent MPEC performance endow the films with a wide range of applications as solid electrolyte membranes.

The importance and impact of the transition toward green energy sources from traditional oil or gasoline-based energy sources becomes more apparent when looking at the amount of expected future energy consumption and the plan to reduce greenhouse gas emissions, primarily CO_2, to protect the climate.[1–3] In this view, the development of stable solid-state electrolytes that can allow simultaneously proton and electron conduction or mixed proton and electron conductivity (MPEC) are desirable in a wide range of practical applications in green energy-related technology, including fuel cells, hydrogen sensors, gas separation, electrolysis and so on. During past years, significant developments in the associated areas are well documented.[4–6] Perovskite oxides and their derivatives (foreign metal atom doped) are widely studied as efficient MPEC materials and the reported proton and electronic conductivities are *ca.* 10^{-2}–10^{-4} and *ca.* 10^{2} S cm^{-1} for proton and electronic conductivity, respectively. However, the high operating temperature of such materials (more than 650 °C) limits their areas of application.[7–10] Therefore, the development of an efficient and stable MPEC that can operate at room temperature will widen the associated application areas.

In fact, some MPEC materials that can operate at room temperature have been reported in recent years.[11–17] These MPEC materials are either (i) heterogeneous mixtures of proton and electron conductors[11–13] or (ii) single-phase mixed proton–electron conductor materials.[14–17] In the former cases, most of the MPEC materials are based on Nafion, which has obvious limitations in terms of very high cost. In addition, mechanical weakness and phase boundary-driven low performance are other drawbacks of such heterogeneous conductors. In the current work, we have demonstrated a stable free-standing thin film prepared from graphene oxide (GO) and oxidized single-wall carbon nanotubes (Ox-SWCNT), GO/Ox-SWCNT, showing excellent MPEC performance.

During the last few decades, GO has been widely studied in almost all areas of science ranging from material science to biological science due to its unique physical and chemical properties including high surface area, high mechanical strength, and so on.[18,19] Significantly, the 2D layer structure of GO consisted of many oxygen-containing functional groups including epoxy, carboxyl, and hydroxyl groups on both sides of the backbone carbon nanosheet allowing it to be modified in the desired dimension.[20] The high proton conductivity of GO is reported in our groups while the oxygen functional group of GO is found to adsorb water in humidified conditions and the proton conduction takes place using the Grotthuss route.[18,21–26] On the other hand, single-wall carbon nanotubes (SWCNTs) are extremely mechanically stable and flexible. They are widely studied 1D carbon allotropes in different areas of application. Hexagonal networks of CNTs consist of shells of carbon atoms that are sp^2-hybridized and responsible for continuous π bonding networks in the CNTs and are favourable for charge transfer including very high electronic conductivity.

[a] *Institute of Industrial Nanomaterials (IINa), Kumamoto University, 2-39-1 Kurokami, Chuo-ku, Kumamoto, 860-8555, Japan. E-mail: hayami@kumamoto-u.ac.jp*
[b] *Department of Chemistry, Graduate School of Science and Technology, Kumamoto University, 2-39-1 Kurokami, Chuo-ku, Kumamoto, 860-8555, Japan*
[c] *National Institute of Advanced Industrial Science and Technology (AIST), Japan*
[d] *Priority Organization for Innovation and Excellence, Kumamoto University, 2-39-1 Kurokami, Chuo-ku, Kumamoto, 860-8555, Japan*
[e] *International Research Center for Agricultural and Environmental Biology (IRCAEB)2-39-1 Kurokami, Chuo-ku, Kumamoto, 860-8555, Japan*

† Electronic supplementary information (ESI) available. See DOI: https://doi.org/10.1039/d2ya00314g

Hatakeyama *et al.* reported single-phase GO-based mixed proton and electron conductivity for the first time.[14] The pristine GO shows considerable proton conductivity, nevertheless, upon reduction of the oxygen functional groups of GO (rGO), some of the sp^3 functionalized C atoms are reduced and restore the graphene-like sp^2 hybridized structure responsible for the electronic conductivity. Therefore, through a controlled reduction process, they optimized the proton and electron conductivity. The obtained proton and electronic conductivities were 1×10^{-4}. Recently, our group has reported the enhanced thermoelectric properties that arise from free-standing GO/CNT membranes.[27] Herein, we are able to obtain a potential mixed proton–electron conductivity using free-standing films of GO and Ox-SWCNT. The oxidization of the SWCNTs is associated with the surface functional groups, which are believed to be involved in the good attachment with GO. The GO is expected to contribute to the proton conduction while the unoxidized part of the Ox-SWCNTs contributes to the electronic conduction part. Moreover, a synergistic effect in the GO/Ox-SWCNT film is expected to improve the overall performance of the resultant materials. For example, the intercalation of Ox-SWCNTs within the GO interlayer inhibits the GO nanosheets from stacking and improves the interlayer spacing favourable for proton conduction in GO/Ox-SWCNT.

SWCNTs were purchased from Zeon Nano Technology Co., Ltd. (ZEONANO^{TM} SG101) and used without further purification. GO and Ox-SWCNT were prepared from the modified hummer oxidation process using pristine graphite powder and SWCNTs, respectively.[18] GO and Ox-SWCNT dispersions were mixed in the ratio (by weight) 1 : 1 and the mixed suspensions were filtered through a membrane using reduced pressure to obtain free-standing GO/Ox-SWCNT membranes. XPS, FTIR, and SEM analyses were employed to characterize the samples. The proton conductivities (impedance) of GO and GO/Ox-SWCNT film (in the out-of-plane direction) were measured by the four-probe AC method using an impedance/gain phase analyser (Solartron 1260) over the frequency range 1 to 10^6 Hz. In a typical cell preparation, each film was cut with a surface area of 1 cm^2. Both sides of the film were covered with gold paste and attached to a gold wire (50 μm diameter, Tanaka Kikinzoku Kogyo). Measurements were executed under controlled temperature and relative humidity (RH) using an incubator (SH-221, ESPEC). Bulk resistances were determined from the radius of the semicircle on the real axis. Proton conductivity (σ) was calculated according to the equation $\sigma = (1/R) \times (d/A)$, where R is the resistance (radius of the semi-circular curve), d is the thickness of the film sample and A is the cross-section area of the sample. On the other hand, to measure the electronic conductivity (from the same measurement cell), the current *versus* voltage curve (I–V curve) was plotted using linear sweep voltammetry while the slope of the I–V curve represents the resistance in Ohm (Ω) of the sample. The electronic conductivity was estimated by the equation of $E = 1/R \times L/A$, where R is the slope of the I–V curve, L is thickness, and A is the area of the film.

The successful surface functionalization of SWCNTs to Ox-SWCNTs during the oxidation process was confirmed from XPS and FTIR spectral analysis. The C 1s XPS spectra of the SWCNTs and Ox-SWCNTs are shown in Fig. S1 (ESI†). A clear difference between the two spectra has been observed. In particular, the characteristic peaks between 286 eV and 288.8 eV are assigned to oxygen containing functional groups including carboxyl groups (–COOH), hydroxyl groups (–C–OH), and epoxy group (C–O–C). In the case of the pristine SWCNTs, the observed peaks in this region are small/insignificant. On the other hand, the appearance of a new peak is observed for the Ox-SWCNTs, which indicates the development of the oxygen functional groups after oxidation.[28] The FTIR spectra of the SWCNTs and Ox-SWCNTs in Fig. S2 (ESI†) further confirm the development of oxygenated functional groups in the Ox-SWCNTs. Compared to the SWCNTs, the appearance of new peaks for the Ox-SWCNTs at 3200–3650 cm^{-1}, 1670–1820 cm^{-1}, and 1050–1150 cm^{-1} can be assigned to the –OH groups, carbonyl (C═O) and C–O functional groups, respectively. The retention of the tubular structure of the SWCNTs after oxidation was confirmed from the SEM images. Fig. 1a and b represent SEM images of the pristine SWCNTs and Ox-SWCNTs, respectively. The tubes of the Ox-SWCNTs are more congested with each other compared to the pristine SWCNTs, which might be due to the interaction among the oxygenated surface functional groups at the Ox-SWCNT surface.

The preparation and characterization of GO from graphite using the modified hummers oxidation process are well-documented in some previous work by our group.[18–22] Therefore, the detailed characterization and properties of pristine GO are not included here. Fig. 1c and d show the optical photographs of free-standing films of GO/Ox-SWCNT prepared using

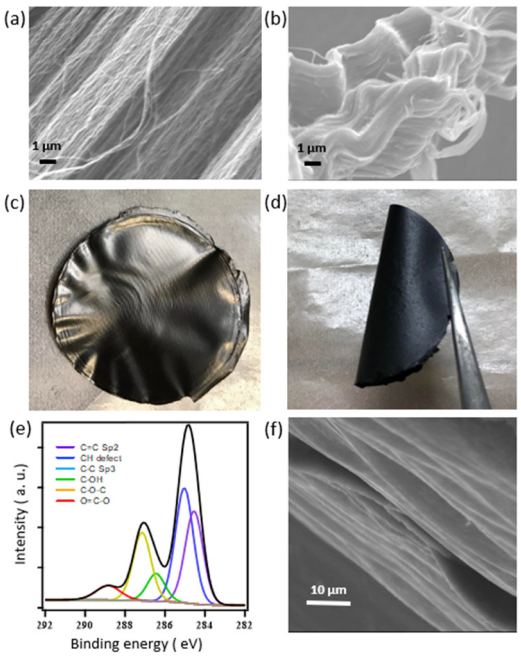

Fig. 1 Surface morphology of the prepared materials. (a) SEM image of SWMCNT, (b) SEM image of Ox-SWCNTs. (c and d) Optical image of the free-standing film of GO/Ox-SWCNT, (e) C 1s XPS spectra of GO/Ox-SWCNT, and (f) cross section SEM images of GO/Ox-SWCNT.

the membrane filter under reduced pressure. The SEM in Fig. S3 (ESI†) shows the distribution of GO and Ox-SWCNTs and demonstrates an excellent attachment of the Ox-SWCNTs to GO. The resultant film is mechanically stable and flexible in nature (Fig. 1d).

The GO/Ox-SWCNT film is believed to be stabilized through noncovalent interaction including van der Waals interactions and hydrogen bonding between GO and the Ox-SWCNTs.[29] Also, no crack in the GO/Ox-SWCNT film is observed after bending the membrane (Fig. S4, ESI†). The C 1s XPS spectra of GO/Ox-SWCNT are shown in Fig. 1e. The XPS survey spectra confirm the oxygen atomic percentage of 20.34% in GO/Ox-SWCNT, which is due to the presence of large oxygen-containing functional groups in GO. Fig. 1f represents the SEM images of the GO/Ox-SWCNT cross-section and the typical layer structure can be confirmed.

The proton and electron conductivity measurements were conducted using the free-standing GO/Ox-SWCNT film at room temperature and 40–100% RH. The mixed conductivity was compared with the pristine GO in the same experimental conditions. The Cole–Cole plots (Nyquist plot) of impedance arising from the GO/Ox-SWCNT film are shown in Fig. S5 (ESI†). The resultant real (Z') *vs.* imaginary parts (Z'') of the impedance observed as distorted semicircular curves followed by the existence of a second circle indicate the characteristic proton conductive properties.[18]

Fig. 2a represents the corresponding proton conductivity values of GO/Ox-SWCNT and GO at room temperature and 40–100%RH. In both cases, the proton conductivity increases gradually with increasing RH, which can be attributed to the enhanced amount of adsorbed water molecules responsible for forming hydrogen bonding for proton transportation. The proton conductivity value increases from 2.24×10^{-6} S cm^{-1} at 40% RH for GO to 7.14×10^{-4} S cm^{-1} at 100% RH. Also, the proton conductivity value increases from 1.25×10^{-5} S cm^{-1} at 40% RH to 5.24×10^{-3} at 100% RH. Clearly, in all conditions, the proton conductivity of GO/Ox-SWCNT shows a higher value than that of pristine GO. Fig. 2b shows the RH-dependent electronic conductivities observed from GO and GO/Ox-SWCNT at room temperature. At 40% RH the electronic conductivity of GO and GO/Ox-SWCNT is 7.81×10^{-6} and 2.05×10^{-3} S cm^{-1}, respectively. The electronic conductivity values of both samples decrease with increasing humidity. At 100% RH conditions, the observed electronic conductivities are 7.81×10^{-6} and 1.35×10^{-3} S cm^{-1}, respectively. The decrease in electronic conductivity with increased RH can be ascribed to the consequence of water uptake. In particular, the adsorption of water results in the swelling of the sample, which in turn disrupted the electronic connections within the carbon structure. The pristine SWCNT shows the electronic conductivity of 1.8×10^{-2} at room temperature and 50% RH in the out-of-plane direction (Fig. S6, ESI†). Compared with the pristine SWCNTs, the lower electronic conductivity of the GO/Ox-SWCNT hybrid can be ascribed to the formation of oxygen functional groups on the SWCNT surfaces with sp^3 hybridized carbon followed by the formation of a hybrid with GO. In particular, the surface functionalization of SWCNTs is

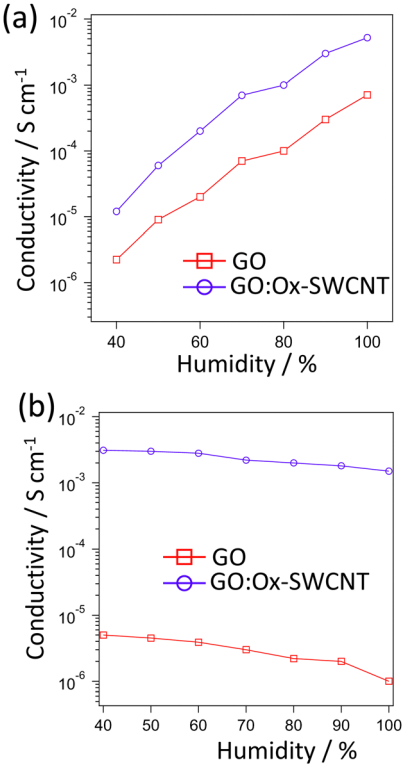

Fig. 2 Mixed conductive properties of GO and GO/OX-SWCNT. (a) Proton conductivity of GO and GO/OX-SWCNT and (b) electronic conductivity of GO and GO/OX-SWCNT.

associated with the certain localization of the conduction electrons of SWCNTs resulting in electronic insulation.

From the above experimental results, the free-standing film of GO/Ox-SWCNT shows considerably high mixed proton and electron conductive properties at room temperature. During past years, GO and related materials have been well studied as proton conductors. The reported out-of-plane proton conductivity of GO is $\sim 10^{-4}$–10^{-3} S cm^{-1} at room temperature and high RH conditions, while showing insignificant electronic conductivity.[18] This high proton conductivity has been ascribed to the presence of oxygen-containing functional groups in the GO surface, including carboxylic acid, hydroxyl, and epoxy groups. Under humidified conditions, GO can adsorb water molecules through oxygenated functional groups, and the proton conduction occurs through the Grotthuss mechanism with continuous breaking and formation of hydrogen bonds.[20] Herein, to achieve a potential mixed conductor from the GO and SWCNT-based materials, the surface of SWCNTs was modified to add polar functional groups by a chemical oxidation process followed by a free-standing film of GO/Ox-SWCNT being prepared through the vacuum filtration process. Interestingly, the addition of Ox-SWCNT on the GO does not interfere with the proton conductivity of the pristine GO; rather GO/Ox-SWCNT shows slightly higher proton conductivity than that of pristine GO. The oxygenated functional groups of CNT arising from hummers oxidation provide a better attachment with GO while facilitating the continuous paths and networks

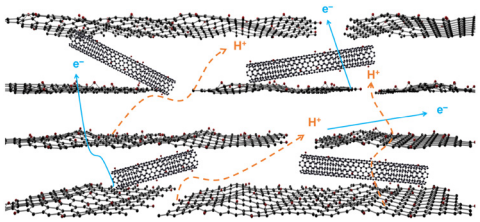

Fig. 3 Proposed mixed proton and electron conducting pathway of GO/Ox-SWCNT.

through H-bonding, which might be attributed to the better proton conductivity in the hybrid. Also, the hydration dynamics are expected to be enhanced due to the generation of interlayer void space of GO due to the addition of Ox-SWCNT in the GO/Ox-SWCNT hybrid.[21] On the other hand, pristine SWCNTs containing a tubular structure of sp^2 hybridized carbon result in a very high electronic conductivity. Upon oxidation, part of the SWCNT surface is oxidized and the non-oxidized part of the SWCNTs with sp^2 hybridized C is expected to show electronic conductivity. Therefore, the GO/Ox-SWCNT hybrid shows a considerable electronic conductivity of 1.35×10^{-3} S cm^{-1}. The proposed mixed proton and electronic conduction route through GO/Ox-SWCNT is shown in Fig. 3.

A number of materials showing room-temperature MPEC properties have been reported in past years. Very recently, Kimura and co-workers reported nickel(III) dithiolene complex/1,4-naphthoquinone as MPEC materials with a proton conductivity of 7.2×10^{-7} S cm^{-1} and electronic conductivity of 4.1×10^{-3} S cm^{-1}.[17] In another study, a mixed proton and electronic conductivity of 3.15×10^{-5} S cm^{-1} and 1.68×10^{-3} S cm^{-1}, respectively, were observed from the oxidized porous carbon.[16] Also, an optimized mixed conductivity for photo-reduced rGO with a proton and electronic conductivity of 1.0×10^{-4} S cm^{-1} was reported.[14] In the current work, we observed a comparable MPEC performance with the existing literature.[11–17] Moreover, the free-standing film with a facile preparation route and enough mechanical stability of the materials signifies their possible practical application as a solid electrolyte membrane.

In summary, we successfully prepared a free-standing film of GO/Ox-SWCNT using a facile route of vacuum filtration under reduced pressure. The material exhibits a considerably high proton conductivity of 5.24×10^{-3} S cm^{-1} and electronic conductivity of 1.35×10^{-3} S cm^{-1}, respectively, at room temperature and 100% RH. The undisturbed flow of ions and charges that arises from the improved attachment of GO and Ox-SWCNT can be attributed to the observed properties. The GO/Ox-SWCNT free-standing film is flexible and mechanically stable, signifying its usefulness in many practical applications including fuel cells, gas separation membranes, and a supercapacitor for room temperature applications.

Conflicts of interest

There are no conflicts to declare.

Acknowledgements

This work was supported by KAKENHI Grant-in-Aid for Scientific Research (A) JP17H01200.

Notes and references

1 N. Abas, A. Kalair and N. Khan, *Futures*, 2015, **69**, 31.
2 N. L. Panwar, S. C. Kaushik and S. Kothari, *Renewable Sustainable Energy Rev.*, 2011, **15**, 1513.
3 M. S. Islam, Y. Shudo and S. Hayami, *Bull. Chem. Soc. Jpn.*, 2022, **95**, 1.
4 M. Papac, V. Stevanović, A. Zakutayev and R. O'Hayre, *Nat. Mater.*, 2021, **20**, 301.
5 B. D. Paulsen, K. Tybrandt, E. Stavrinidou and J. Rivnay, *Nat. Mater.*, 2020, **19**, 13.
6 B. P. Tripathi, M. Schieda, V. K. Shahi and S. P. Nunes, *J. Power Sources*, 2011, **196**, 911.
7 D. R. Rolison, P. L. Hagans, K. E. Swider and J. W. Long, *Langmuir*, 1999, **15**, 774.
8 S. Escolastico, S. Somacescu and J. M. Serra, *Chem. Mater.*, 2014, **26**, 982.
9 S. Escolástico, C. Solis, T. Scherb, G. Schumacher and J. M. Serra, *J. Membr. Sci.*, 2013, **444**, 276.
10 T. Sakai, K. Isa, M. Matsuka, T. Kozai, Y. Okuyama, T. Ishihara and H. Matsumoto, *Int. J. Hydrogen Energy*, 2013, **38**, 6842.
11 A. Boldeiu, E. Vasile, R. Gavrila, M. Simion, A. Radoi, A. Matei, I. Mihalache, R. Pascu and M. Kusko, *Colloids Surf., A*, 2014, **461**, 133.
12 M. Tortello, S. Bianco, V. Ijeri, P. Spinelli and E. Tresso, *J. Membr. Sci.*, 2012, **415–416**, 346.
13 B. A. Aragaw, W.-N. Su, J. Rick and B.-J. Hwang, *RSC Adv.*, 2013, **3**, 23212.
14 K. Hatakeyama, H. Tateishi, T. Taniguchi, M. Koinuma, T. Kida, S. Hayami, H. Yokoi and Y. Matsumoto, *Chem. Mater.*, 2014, **26**, 5598.
15 K. Hatakeyama, M. S. Islam, K. Michio, C. Ogata, T. Taniguchi, A. Funatsu, T. Kida, S. Hayami and Y. Matsumoto, *J. Mater. Chem. A*, 2015, **3**, 20892.
16 M. S. Islam, M. R. Karim, N. N. Rabin, R. Ohtani, M. Nakamura and S. Hayami, *Chem. Lett.*, 2017, **46**, 1828.
17 Y. Kimura, Y. Yoshida, M. Maesato and H. Kitagawa, *Chem. Lett.*, 2021, **50**, 439.
18 M. R. Karim, K. Hatakeyama, T. Matusi, H. Takehira, T. Taniguchi, M. Koinuma, Y. Matsumoto, T. Akutagawa, T. Nakamura, S. Noro, T. Yamada, H. Kitagawa and S. Hayami, *J. Am. Chem. Soc.*, 2013, **135**, 8097.
19 M. Fukuda, M. S. Islam, R. Shimizu, H. Nassar, N. N. Rabin, Y. Takahashi, Y. Sekine, L. F. Lindoy, T. Fukuda, T. Ikeda and S. Hayami, *ACS Appl. Nano Mater.*, 2021, **4**, 11881–11887.
20 M. R. Karim, K. Hatakeyama, M. Koinuma and S. Hayami, *J. Mater. Chem. A*, 2017, **5**, 7243.
21 M. R. Karim, M. S. Islam, K. Hatakeyama, M. Nakamura, R. Ohtani, M. Koinuma and S. Hayami, *J. Phys. Chem. C*, 2016, **120**, 21976.
22 K. Wakata, M. S. Islam, M. R. Karim, K. Hatakeyama, N. N. Rabin, R. Ohtani, M. Nakamura, M. Koinuma and S. Hayami, *RSC Adv.*, 2017, **7**, 21901.
23 M. R. Karim, M. S. Islam, N. N. rabin, R. Ohtani, M. Nakamura, M. Koinuma and S. Hayami, *Aust. J. Chem.*, 2016, **70**, 642.

24 M. Fukuda, M. S. Islam, Y. Shudo, J. Yagyu, L. F. Lindoy and S. Hayami, *Chem. Commun.*, 2020, **56**, 4364.
25 K. Wakata, M. R. Karim, M. S. Islam, R. Ohtani, M. Nakamura, M. Koinuma and S. Hayami, *Chem. – Asian J.*, 2017, **12**, 194.
26 J. Yagyu, Md. S. Islam, Y. Shudo, M. Fukuda, H. Ushijima, J. Ohyama, S. Ida, L. F. Lindoy and S. Hayami, *ACS Appl. Energy Mater.*, 2021, **4**, 6296.
27 M. S. Islam, H. Ohmagari, M. A. Rahman, M. Fukuda, Y. Shudo, J. Yagyu, Y. Sekine, L. F. Lindoy and S. Hayami, *Mater. Adv.*, 2021, **2**, 5645.
28 Y. Matsumoto, M. Koinuma, S. Y. Kim, Y. Watanabe, T. Taniguchi, K. Hatakeyama, H. Tateishi and S. Ida, *ACS Appl. Mater. Interfaces*, 2010, **2**, 3461.
29 M. Musielak, A. Gagor, B. Zawisza, E. Talik and R. Sitko, *ACS Appl. Mater. Interfaces*, 2019, **11**, 28582.